Brazilian Journal of Chemical Engineering
https://doi.org/10.1007/s43153-023-00406-y

ORIGINAL PAPER

Synthesis and characterization of Cu-rGO/ZnO nanocomposite for photocatalytic degradation of bromophenol blue and antibacterial activity

S. Rajakumari[1,2] · **S. Mohandoss**[2] · **S. Sureshkumar**[2]

Received: 21 March 2023 / Revised: 14 September 2023 / Accepted: 16 September 2023
© The Author(s) under exclusive licence to Associação Brasileira de Engenharia Química 2023

Abstract
Herein, Cu-rGO/ZnO ternary nanocomposite powder was synthesized by the hydrothermal method. Analytical techniques such as X-ray diffraction (XRD), Fourier transform infrared (FTIR), Ultraviolet and visible (UV–Vis), Scanning electron microscopy-energy dispersive X-ray analysis (SEM–EDX), Brunauer–Emmett–Teller (BET) and X-ray photoelectron spectroscopy (XPS) were used to study morphology and structural properties of the obtained nanocomposite. The photocatalytic activity of the synthesized Cu-rGO/ZnO ternary nanocomposite was assessed by the degradation of bromophenol blue in aqueous media (pH 7.4). The photocatalytic results demonstrated that the Cu-rGO/ZnO ternary nanocomposite photocatalyst (0.1 g/L) exhibited 86.21% degradation of 10 ppm bromophenol blue dye at 150 min by using the Xe arc lamps, 20 W (with ultraviolet cut-off filter). Band gap widening by Cu doping and efficient electron hole separation induced by rGO were responsible for enhanced photocatalytic activity. The antibacterial test results revealed that the Cu-rGO/ZnO nanocomposite exhibited significant antibacterial activity against Escherichia coli, Staphylococcus aureus, Enterococcus faecium and Pseudomonas aeruginosa.

Keywords Cu-rGO/ZnO · Photocatalyst · Dye degradation · Antibacterial activity

Introduction

The photocatalysts based on nano metal oxides has been gaining much attention for environmental applications (Kumar and Chawla 2014; Ganachari et al. 2019; Jagadeeshan and Parsanathan 2019). The advanced oxidation process has emerged as a novel technique for the degradation of organic and inorganic pollutants from waste water. Advanced oxidation process exploit highly reactive transitory species (H_2O_2, $OH^{\cdot}$, $O_2^{\cdot -}$, O_3) in the oxidation process and degrade pollutants. Among advanced oxidation processes, semiconductor based heterogenous photocatalysis has been used prominently for water treatment. Heterogenous photocatalysis removes pollutants from waste water by generating hydroxyl radicals and transforming them into less toxic organic compounds. Mostly, the heterogeneous photocatalyst has been recognized as a promising material for removal of organic pollutants from aqueous solution (Silva and Faria 2009). Bromophenol blue is used as a pH indicator and most importantly used in gel electrophoresis as a tracking dye. However, the release of such an organic pollutant into the environment leads to various toxic effects in living organisms (Chiam et al. 2020). Several techniques such as membrane filtration, reverse osmosis, ion exchange, and photocatalysis have been developed for wastewater treatment (Bayramoglu et al. 2020; Chadha et al. 2022; Zhang et al. 2018). Among them, photocatalysis has emerged as a powerful and easy technique for organic pollutant removal from aqueous media (Mohamed and Mohamed 2018). Several nano metal oxides such as TiO_2, WO_3, ZnO, SnO_2, are excellent photocatalysts under visible or ultraviolet irradiation (Danish et al. 2021; Arora et al. 2016; Gautam et al. 2020). Among them, ZnO based binary and ternary nanocomposites have been considered an excellent photocatalysts for organic dye degradation in aqueous solution due to their excellent physicochemical properties, low cost, high thermal stability, environmentally friendly and easy preparation (Ullah et al.

✉ S. Rajakumari
rajakumarisubramaniyan1981@gmail.com

[1] Department of Chemistry, Gojan School of Business and Technology, Chennai, Tamil Nadu, India

[2] Department of Chemistry, Rajalakshmi Engineering College, Chennai, Tamil Nadu, India

Published online: 09 October 2023

Jul. 2021; Pirhashemi et al. 2018; Sureshkumar et al. 2019; Jothimani et al. 2017). However, ZnO possesses a wide band gap (3.4 eV), has high binding energy at room temperature (60 meV), and has poor electron mobility (115–155 cm^{-2} V^{-1} S^{-1}) which limits its use in many industrial applications (Janotti and Walle 2009). Efforts have been made to narrow down the band gap and to prevent electron hole pair recombination by combining ZnO with other functional materials such as reduced graphene oxide (rGO), carbon nanotubes and graphite (Mohammad et al. 2018; Sampaio et al. 2015; Kumar et al. 2018; Dědková et al. 2015; Balasubramani et al. Jun. 2019). The binary composite based on ZnO/rGO has been developed for photocatalytic applications (Sengunthar et al. 2020; Bolaghi et al. 2019; Xue and Zou 2018; Ramos et al. 2019; Peng et al. 2015; Wu et al. 2016). Non-uniform distribution and agglomeration are challenging during the preparation of binary composite materials based on rGO/ZnO for photocatalytic application. To overcome such a challenge, transition metal ions such as Cu are used to dope the rGO/ZnO binary composites (Asgharian et al. 2019). Synthesis of copper and graphene activated ZnO nanocomposite powders by wet chemical method for enhanced photocatalytic activity has been reported. It was found that Cu doped rGO/ZnO nanopowder exhibits excellent photocatalytic activity of degradation of methylene blue (Ravichandran et al. 2016). Shu-Han Hsieh et al. prepared ternary Cu-doped ZnO/Graphene materials for methylene blue degradation. The copper doping serves to enhance the visible light response due to the resulting ZnO bandgap narrowing and the rGO functions to reduce recombination due to the excellent electrical conductivity of the rGO (Hsieh and Ting 2018). Sulakshana Shenoy et al. reported on the synthesis of copper doped zinc oxide grafted on graphene layers for visible light driven photocatalysts (Shenoy et al. 2021).

Exploration of Cu-rGO/ZnO nanocomposite for bromophenol blue degradation is not yet reported. Thus, in the present study, a Cu-rGO/ZnO ternary nanocomposite was synthesized for photocatalytic and antibacterial activity. The prepared composite was characterized using XRD, SEM, EDAX, FTIR, UV–Vis, BET, and XPS to elucidate the structural and morphological properties. Photocatalytic activity of the composite material was investigated by the degradation of bromophenol blue under ultraviolet light irradiation. The antibacterial activity of the prepared sample was evaluated by the Agar well diffusion method against common pathogenic bacterial strains.

Experimental

Materials

The following chemicals zinc acetate dihydrate extra pure AR 99.5%, 98% H_2SO_4, graphite oxide powder 98% assay, Sodium hydroxide extra pure AR 98%, sodium nitrate extra pure AR ACS 99%, Cupric Acetate Monohydrate pure 98% and Potassium Permanganate extra pure AR 99.5% were procured from SRL chemicals. Deionized water (DI water) was used throughout the experiments. All other necessary chemicals and reagents used in the experiment were of analytical grade and used without further purification.

Preparation of ZnO nanoparticles

The undoped ZnO was prepared by a facile hydrothermal method. For ZnO preparation, Zinc acetate dihydrate (0.1 M), and Cetyltrimethylammonium bromide (0.01 M) were mixed in a 250 ml glass beaker and stirred for 10 min to obtain a homogenous solution. The pH of the obtained reaction mixture was increased to 9 by adding 1 M NaOH. The whole reaction mixture was carefully transferred to Teflon lined stainless steel autoclave and kept at 130 °C for 3 h. The obtained precipitate was thoroughly washed with DI water, followed by ethanol to eliminate unwanted impurities. The obtained ZnO precipitate was then centrifuged, dried at 70 °C, sintered at 350 °C for 2 h and stored in a clean glass vial for further studies.

Preparation of graphene oxide

Graphene oxide (GO) was prepared using the Modified Hummer's method (Hummers and Offeman 1958). Briefly, 27 ml of sulphuric acid and 3 ml of phosphoric acid were gently mixed and stirred for 10 min. Then, 0.250 g of graphite powder was added to the above mixture with constant stirring. 1.5 g of $KMnO_4$ was added to the above reaction mixture while maintaining the temperature at less than 20 °C to prevent an explosion. The whole reaction mixture was continuously stirred at 32 °C for 24 h. Then, the reaction mixture was diluted to 500 ml of deionized water under vigorous stirring. To remove excess $KMnO_4$, 30% H_2O_2 was added slowly and stirred for 15 min. The obtained precipitate was washed with 5% HCl acid and deionized water and centrifuged at 6000 rpm for 10 min. The resultant precipitate was dried in an oven at 90 °C for 24 h to obtain graphene oxide.

Preparation of the photocatalyst (Cu-rGO/ZnO)

The GO suspension was prepared by adding GO (1.5 g) into distilled water and a few drops of N_2H_4 (6 drops) were added under constant stirring. Zinc acetate dihydrate (0.1 M), Cetyltrimethylammonium bromide (0.01 M) and 0.01 M solution of cupric Acetate Monohydrate were taken in a separate beaker and stirred for 15 min. To this solution, GO suspension was added gradually and stirred for 20 min. The pH of the reaction mixture was adjusted to 9 by adding 1 M

NaOH solution under constant stirring. Finally, the reaction mixture was transferred to a Teflon-lined stainless steel autoclave and kept at 130 °C for 3 h. The obtained precipitate was centrifuged and washed with DI water followed by ethanol to get an impurities-free catalyst. After that, the obtained material was dried at 70 °C, sintered at 350 °C for 2 h in a muffle furnace with air contact and denoted as Cu-rGO/ZnO nanocomposite. The percentage ratio of each component in the catalyst Cu-rGO/ZnO nanocomposite is 0.1:10:1 respectively. A similar protocol was followed for preparing rGO/ZnO without adding cupric acetate monohydrate to compare the efficiency of the Cu-rGO/ZnO composite.

Characterization of Cu-rGO/ZnO nanocomposite

The structure and the morphological properties of the prepared catalyst were studied using X-ray diffraction (XRD), scanning electron microscopy (SEM), Energy Dispersive X-ray (EDX) analysis, and Fourier Transform Infrared Spectroscopy (FTIR) analytical techniques. The XRD patterns were recorded using a D-8 Advance Bruker AXS diffractometer with Cu Ka radiation (λ = 1.5406 Å). The FTIR spectra of the prepared Cu-rGO/ZnO nanocomposite were analyzed using the FT-IR (Jasco FT/IR-4600 type A, range: 400–4000 cm^{-1}, Detector-TGS using KBr pellets). UV–Visible spectra for samples were obtained by UV–Visible spectrophotometer (HITACHI). Photoluminescence of the samples were analyzed by an Agilent-Cary eclipse spectrophotometer (Model: FL1201M002). BET (Brunauer, Emmett and Teller) analysis was carried out to determine the surface area and the pore size of the composite on the instrument Quantachrome® ASiQwin™ Instrument version 5.0. The sample's surface chemical state was analysed using X-ray photoelectron spectroscopy (XPS, ThermoFisher Scientific ESCALAB250Xi). The pH of point of zero charge (pH_{PZC}) for the sample was measured as follows, each catalyst was added into aqueous solution. The pH of the mixture was adjusted to 2–12 using 0.1 M HCl and 0.1 M NaOH and kept at inert atmosphere for 48 h, initial (pH_i) and final (pH_f) pH was measured. The difference between initial (pH_i) and final (pH_f) values ($\Delta pH = pH_i - pH_f$) (Y-axis) was plotted against the initial pH_i (X axis). The intersection provides the pH_{PZC} values for each catalyst.

Photocatalytic study

The photocatalytic performance of the prepared nanocomposite was evaluated by photocatalytic degradation of bromophenol blue under UV light in a photocatalytic chamber. The sample Cu-rGO/ZnO was added to the aqueous solution of bromophenol to determine the photocatalyst effect. The Xe arc lamps, 20 W (with ultraviolet cut-off filter), were utilized as a light source. The bromophenol blue (10 ppm) aqueous solution was prepared for each experiment, and a known amount of photocatalyst was dispersed. The suspension (bromophenol blue with photocatalyst) was ultrasonicated for 20 min in a dark room at ambient temperature. The pH = 7.4 was observed during the degradation test. All experiments were conducted at ambient conditions for 150 min, and all samples were filtered and centrifuged to eliminate the photocatalyst substance. A UV–Vis double beam spectrophotometer (HITACHI, Model: UH5300) was used to measure the UV–Vis absorbance of samples.

Photocatalytic degradation of bromophenol blue dye solution by the synthesized samples were investigated under Xe arc lamps, 20 W (ultraviolet cut-off filter) with irradiation

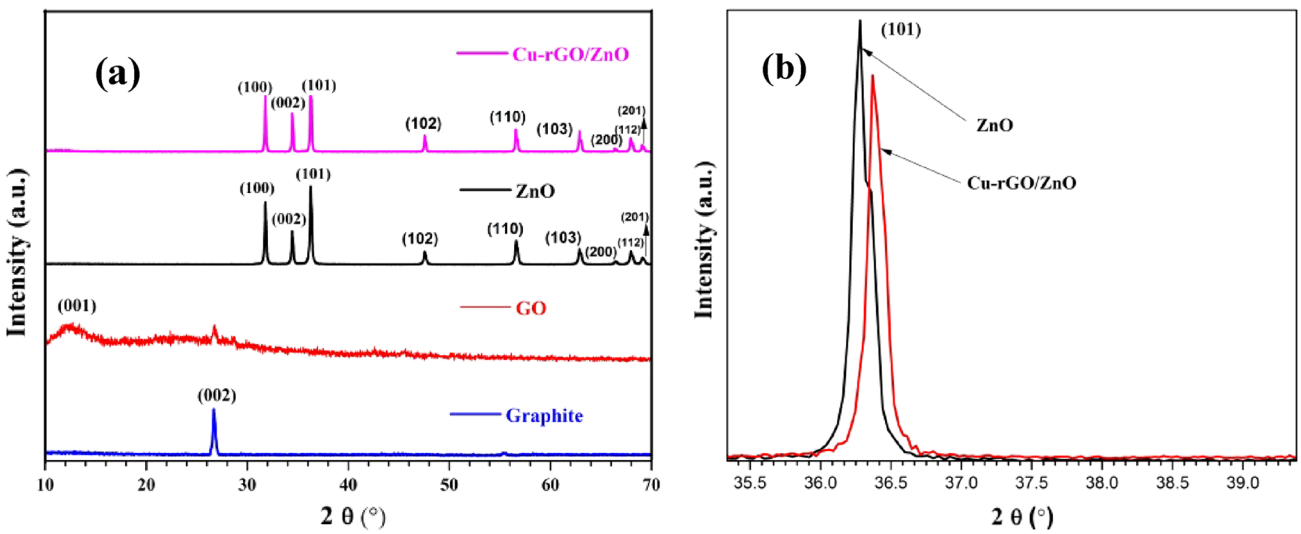

Fig. 1 X-ray diffraction pattern of **a** graphite, GO, ZnO, and Cu-rGO/ZnO nanocomposite **b** displacement XRD peaks of ZnO and Cu-rGO/ZnO

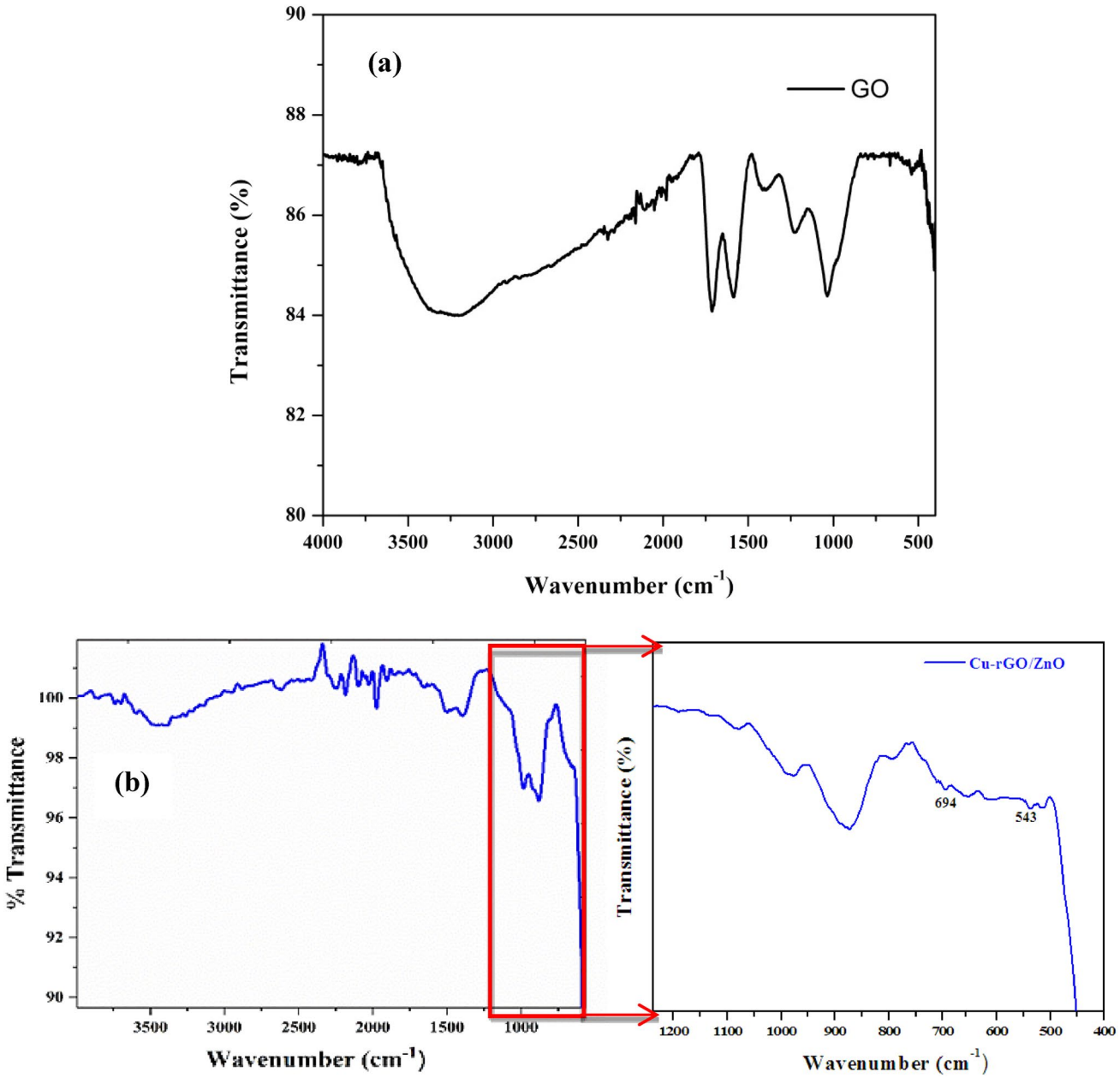

Fig. 2 FTIR spectra obtained for **a** graphene oxide and **b** Cu-rGO/ZnO nanocomposite

wavelength 365 nm. The degradation efficiency of the synthesized photocatalysts was calculated using the following equation.

$$\text{Degradation efficiency} = \frac{C_o - C_t}{C_o} \times 100$$

where C_o is the absorbance of the pollutant (bromophenol blue) before the photo irradiation and C_t is the absorbance of the pollutant (bromophenol blue) after time t min.

Antibacterial activity

The antibacterial activity of Cu-rGO/ZnO nanocomposite was tested by using the agar well diffusion method. For the study of antibacterial activity, the following gram-positive and gram-negative bacterial strains have been used. Gram-positive bacteria: *Enterococcus faecium* and *Staphylococcus*

aureus. Gram-negative bacteria: *Escherichia coli* and *Pseudomonas aeruginosa*. Bacterial strains (24 h old) were spread on agar plates, where the bacterial cell density was 106 CFU/mL. The agar well was made using a sterile borer. Different concentrations of nanocomposites (50 µg/mL, 100 µg/mL, 150 µg/mL, and 200 µg/mL) were added to the wells and inoculated plates were incubated at 35 °C for 24 h. Then the zone of inhibition was measured on the mm scale.

Results and discussion

XRD analysis

Structural properties and reduction of as-prepared GO into rGO on the nanocomposite can be verified by XRD analysis. The XRD pattern of graphite, graphene oxide, ZnO and Cu-rGO/ZnO nanocomposites has been shown in Fig. 1a. The XRD pattern of graphite shows the characteristic peak

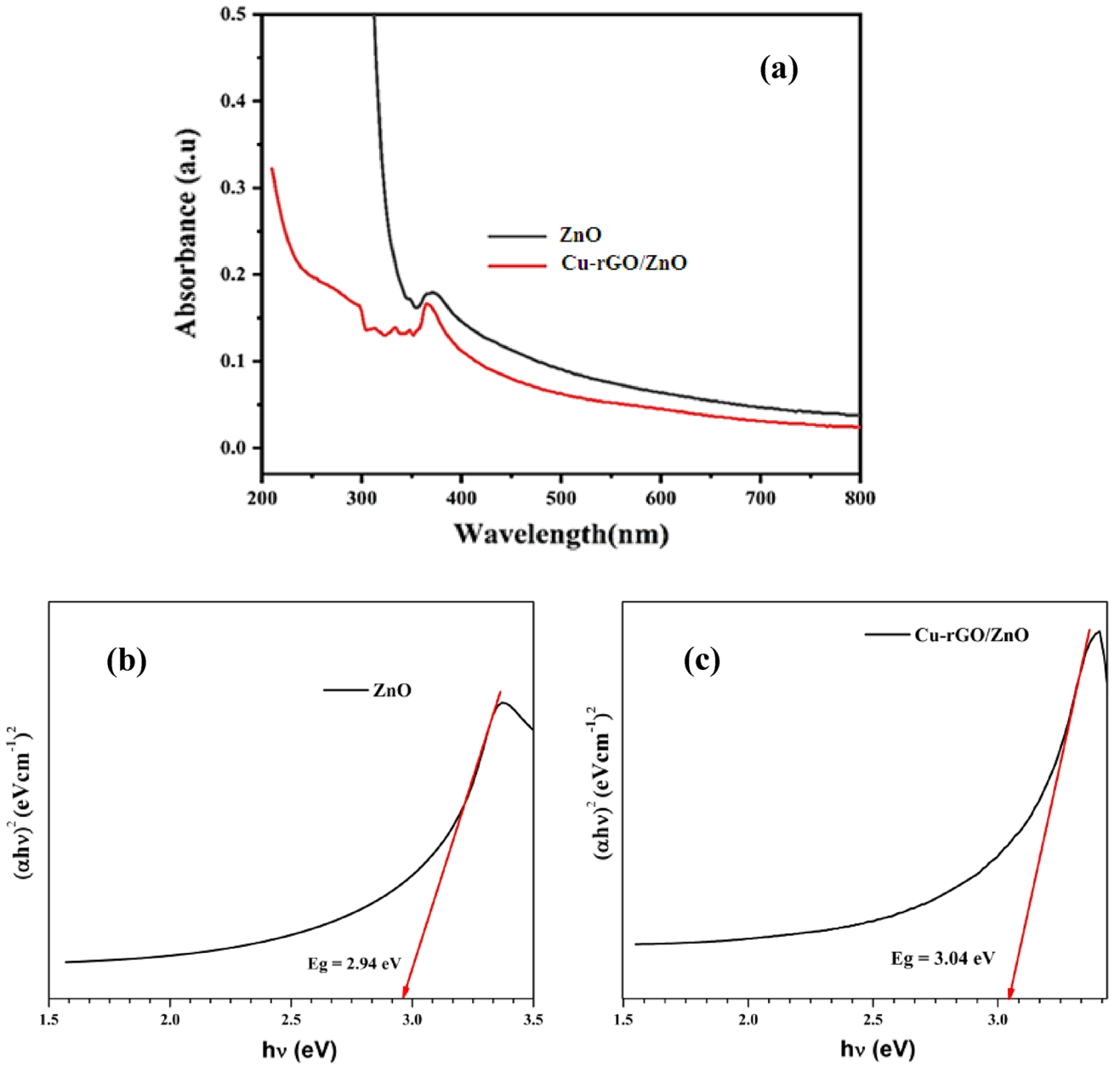

Fig. 3 **a** UV–Visible spectra of ZnO and Cu-rGO/ZnO nanocomposite, **b** Tauc plot of ZnO nanoparticles **c** Tauc plot of Cu-rGO/ZnO nanocomposite

(002) at 2θ = 26.5° (JCPDS 75-2078). The XRD pattern of GO shows the characteristic peak at 2θ = 10.22, indicating that the graphite is converted into graphene oxide and subsequently exfoliated upon oxidation. Further, the XRD pattern of GO shows additional diffraction peak appeared at 2θ = 26.5° is due to the unoxidized graphite portion. As observed from Fig. 1a, the XRD pattern of the ZnO sample showed hexagonal (wurtzite) phase which is consistent with standard JCPDS card No 36–1451. The diffraction pattern of Cu-rGO/ZnO nanocomposites in which the diffraction peaks appearing at 31.7°, 34.2°, 36.3°, 47.6°, 56.6°, 62.8°, 67.8° and 69.3° are attributed to the (100), (002), (101), (102), (110), (103) and (112) and (201) planes, respectively, and exhibit the hexagonal (wurtzite) phase of ZnO. The diffraction patterns are in agreement with JCPDS card no 36–1451. Results indicate that the Cu^{2+} ion and rGO did not change the crystalline structure of ZnO. The diffraction peaks belonging to rGO (2θ values of 24.6 and 43.3) were not observed in the XRD patterns of nanocomposite (Cu-rGO/ZnO), which might be produced by the limited amount of rGO. In addition to that, the surface of rGO is fully covered by ZnO nanoparticles. Similar results were already reported in previous research articles (Gang et al. 2021; Mohammad et al. 2017). Similarly, no additional peaks related to Cu were observed in the diffraction pattern, which inferred that Cu^{2+} ions substituted at the ZnO crystal lattice at the Zn^{2+} sites. The substitution is achieved due to the fact that the ionic radii of Cu^{2+}(0.73 Å) is close to that of Zn^{2+} (0.74 Å) (Meshram et al. 2016). The crystallite size was calculated using the Scherrer equation. According to the Scherrer formula, the average crystallite size was found to be 54 nm for ZnO and 48 nm for Cu-rGO/ZnO.

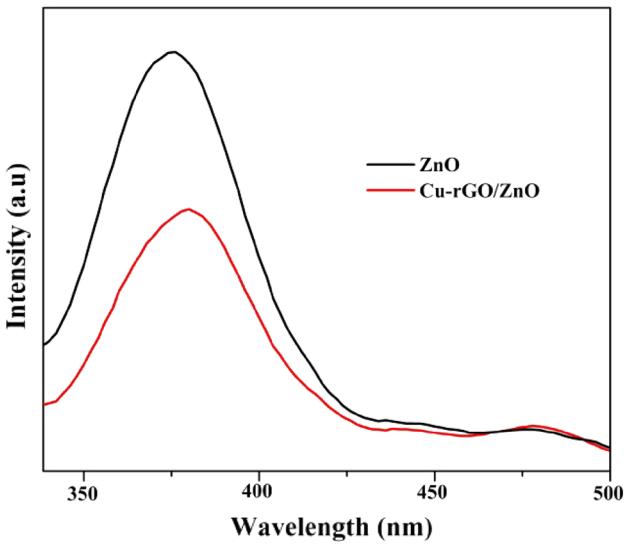

Fig. 4 PL spectra of ZnO and Cu-rGO/ZnO nanocomposite with an excitation at 350 nm

Figure 1b shows the XRD peaks displacement of Cu-rGO/ZnO and ZnO. It is observed that the diffraction pattern of Cu-rGO/ZnO slightly shifted to a higher angle when compared to ZnO, indicating the successful doping of Cu ions into the ZnO crystal structure. The results are in agreement with previous studies (Srinet et al. 2013; Herng et al. Jan. 2007). The lattice constant for Cu-rGO/ZnO and ZnO was calculated by Rietveld refinement and are found to be a = 3.2476 Å, c = 5.1955 Å and a = 3.2512 Å, c = 5.2071 Å respectively. The decrease in lattice constant is due to the substitution of Cu^{2+} into the Zn^{2+} crystal structure.

FTIR analysis

Fourier transform infrared (FTIR) spectroscopy was carried out to determine the functional groups present in the prepared nanocomposites. FTIR also reveals the presence of impurities on the sample surface.

Figure 2a shows the FTIR spectra of graphene oxide. The broad peak is observed at 3328 cm^{-1} indicating the O–H stretching mode of the carboxyl group present in GO (Zhang and Zhang 2011; Guo et al. Sep. 2009). The peaks observed at 2925 cm^{-1} and 2828 cm^{-1} are due to the asymmetric and symmetric CH_2 stretching of graphene oxide respectively. The peak 1612 cm^{-1} indicates the C = C stretching vibration of unoxidized graphite (Asgharian et al. 2019). The peak at 1720 cm^{-1} is attributed to the C = O stretching of a carboxyl group. The peak at 1226 cm^{-1} is attributed to the C–OH stretch of the alcohol group while the peak at 1062 cm^{-1} is attributed to C–O stretching vibrations of C–O–C. Figure 2b shows the FTIR spectra of CTAB-capped Cu-rGO/ZnO nanocomposites. The peak at 543 cm^{-1} is assigned to Zn–O stretching vibrations and the two weak bands observed at 694 and 874 cm^{-1} indicate that Cu ions are incorporated into the ZnO lattice site (Baizaee et al. 2018; Thennarasu and Sivasamy 2016). The peaks at 1023 cm^{-1}, 1395 cm^{-1}, 1456 cm^{-1}, and 1535 cm^{-1}, are related to alkoxy (C–O) stretching vibration, epoxy (C–O–C) stretching vibration, deformation of a carboxylic group (–OH), aromatic carbon–carbon double bond stretching (C = C) in graphene respectively. The peak at 1659 cm^{-1}, is related to carbon–carbon double bond vibration (C = C) due to unoxidized graphene parts. The peak at 1742 cm^{-1} is due to carbonyl (C = O) reduction in GO (Asgharian et al. 2019).

UV–visible spectroscopy

Absorption spectroscopy is a non-destruction technique to elucidate the optical properties of nanoparticles. The UV–Visible absorption spectra were obtained for the

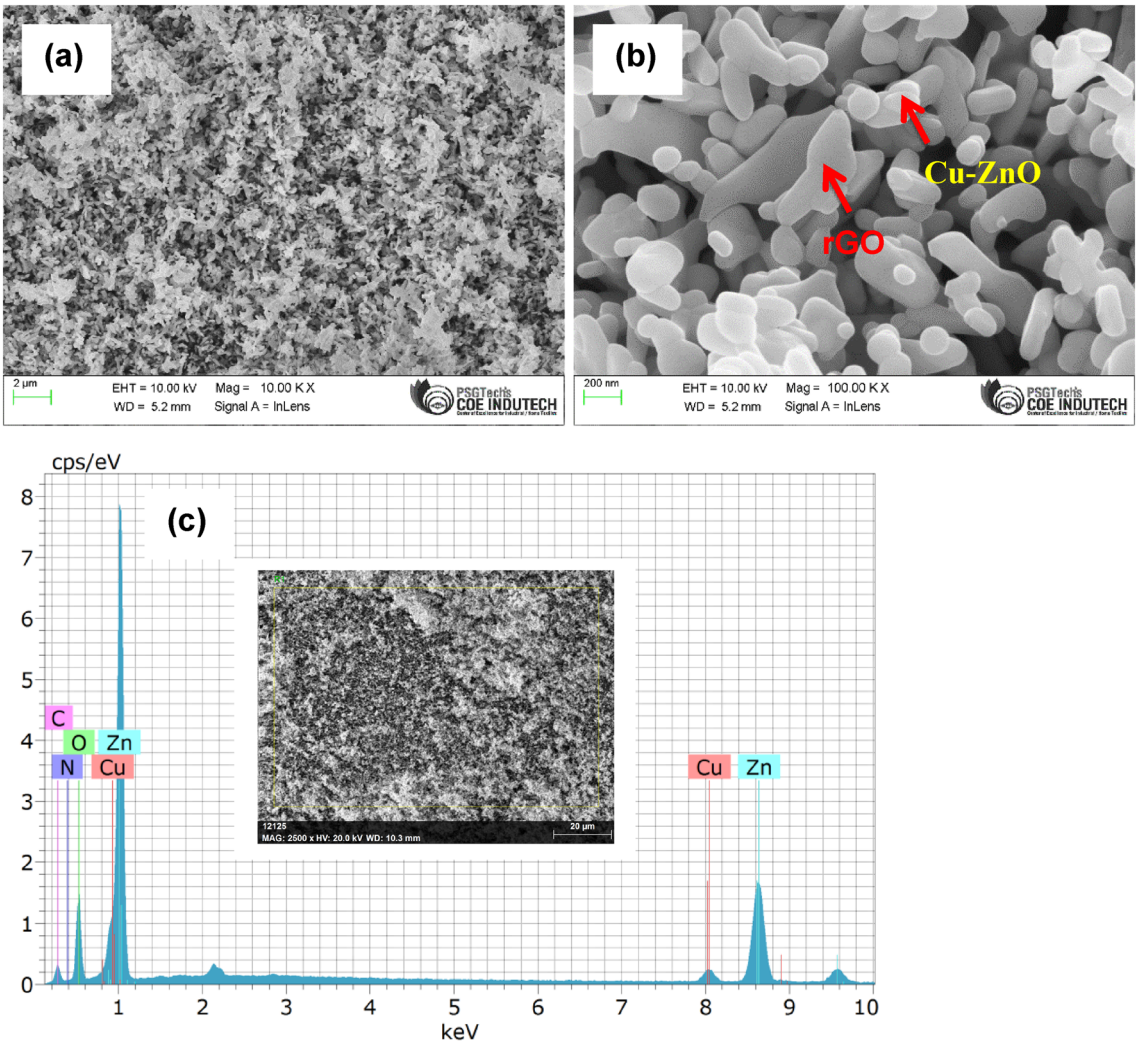

Fig. 5 SEM image of **a** low magnification of Cu-rGO/ZnO nanocomposite, **b** high magnification of Cu-rGO/ZnO nanocomposite, and **c** EDAX obtained for Cu-rGO/ZnO nanocomposite

Table 1 Elemental composition of Cu-rGO/ZnO nanocomposite

Element	Wt (%)	At. (%)
Zinc	64.97	31.23
Oxygen	22.31	34.97
Carbon	11.58	31.51
Copper	1.13	2.27

samples within the wavelength range of 200 nm to 800 nm. The UV–Visible absorption spectra result of ZnO and the Cu-rGO/ZnO nanocomposite are presented in Fig. 3. It signifies that the maximum absorption observed at 374 nm and 368 nm for ZnO and the Cu-rGO/ZnO nanocomposite is due to the large exciton binding energy of the bulk ZnO at room temperature. The slight blue shift that is observed for the Cu-rGO/ZnO nanocomposite is due to the quantum confinement effect among individual nanoparticles, indicating that the size of the CTAB-capped Cu-rGO/ZnO is small (48 nm) when compared to pure ZnO (54 nm) nanoparticles (Bramhaiah et al. 2016; Khurshid et al. Feb. 2019). The optical band gap of the prepared samples was calculated using the Tauc relation, $\alpha h\nu = A(h\nu - Eg)1/2$, where A is a constant, Eg is the bandgap energy of the sample and 1/2 defines the direct allowed transition. Figure 3b, c shows the Tauc plot obtained for ZnO and Cu-rGO/ZnO nanocomposite. The band gap energy (Eg) is calculated as 2.94 eV and 3.04 eV for ZnO and the Cu-rGO/ZnO nanocomposite respectively, indicating the band gap energy (3.04 eV)

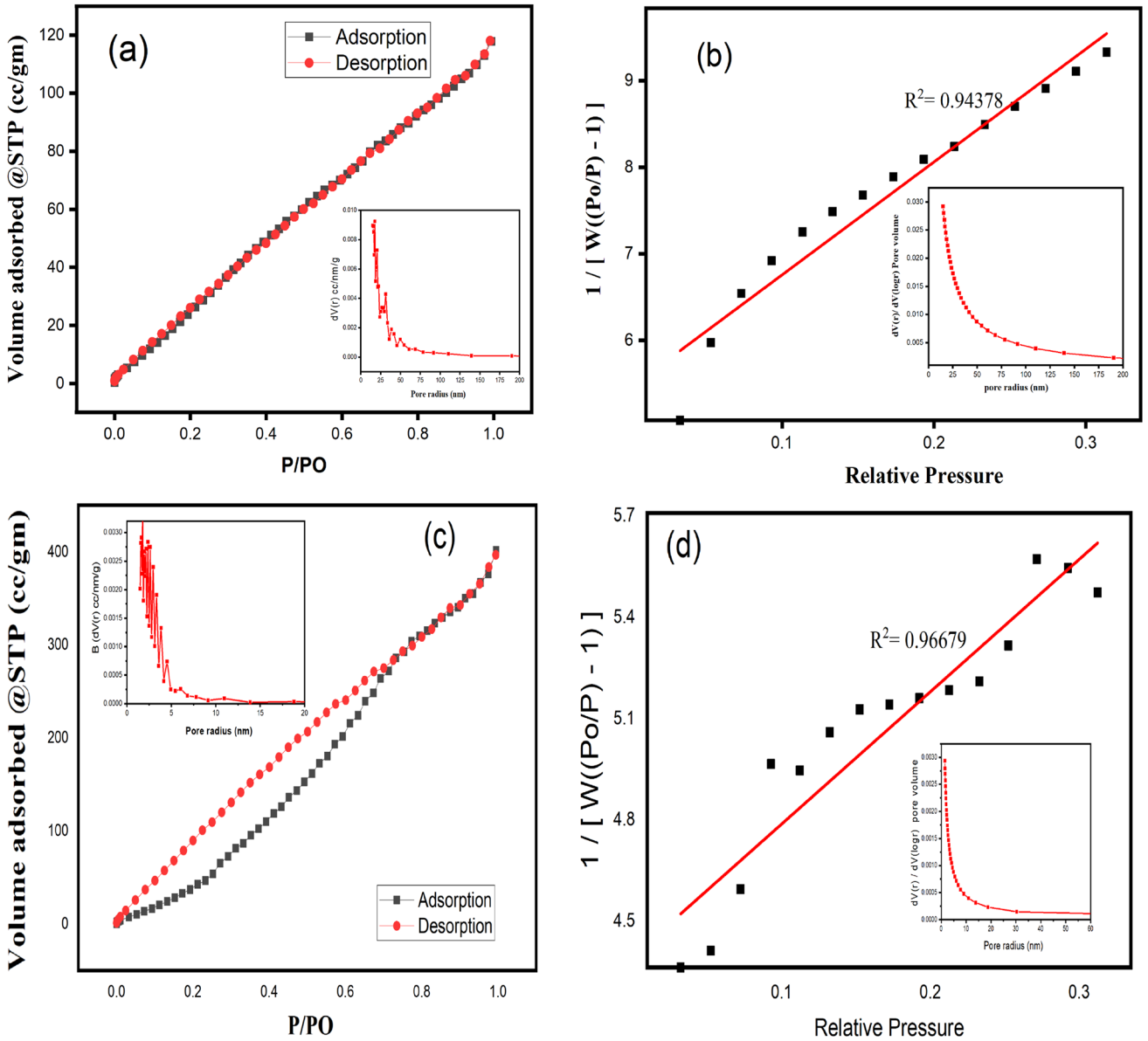

Fig. 6 **a** BET analysis of nitrogen adsorption–desorption isotherm and pore-size distribution curve ZnO nanoparticles. **b** The plot of 1/[(W(Po/P)−1)] and relative pressure for surface area calculation of ZnO nanoparticles. **c** BET analysis of nitrogen adsorption–desorption isotherm and pore-size distribution curves (inserted images) of Cu-rGO/ZnO nanocomposite, **d** the plot of 1/[(W(Po/P)−1)] and relative pressure for surface area calculation of Cu-rGO/ZnO nanocomposite

widened due to the addition of Cu^{2+} and rGO. The addition of Cu and rGO can create more oxygen vacancies in the ZnO surface. Similar results also observed in published literatures (Kavitha et al. 2015; Sernelius et al. Jun. 1988; Vink et al. Oct. 1996; Etacheri et al. May 2012). The interrelation of particle size and band gap energy can give an understanding of photocatalytic characteristics of ZnO and the Cu-rGO/ZnO nanocomposite.

Photoluminescence

Photoluminescence (PL) analysis was carried out to elucidate the mechanism behind the transfer process of photo-induced electron–hole pairs and the role of defects in the prepared photocatalyst (Mandal et al. 2019). The PL spectra of ZnO and Cu-rGO/ZnO are shown in Fig. 4. It is well known that the stronger intensity of PL emission indicates

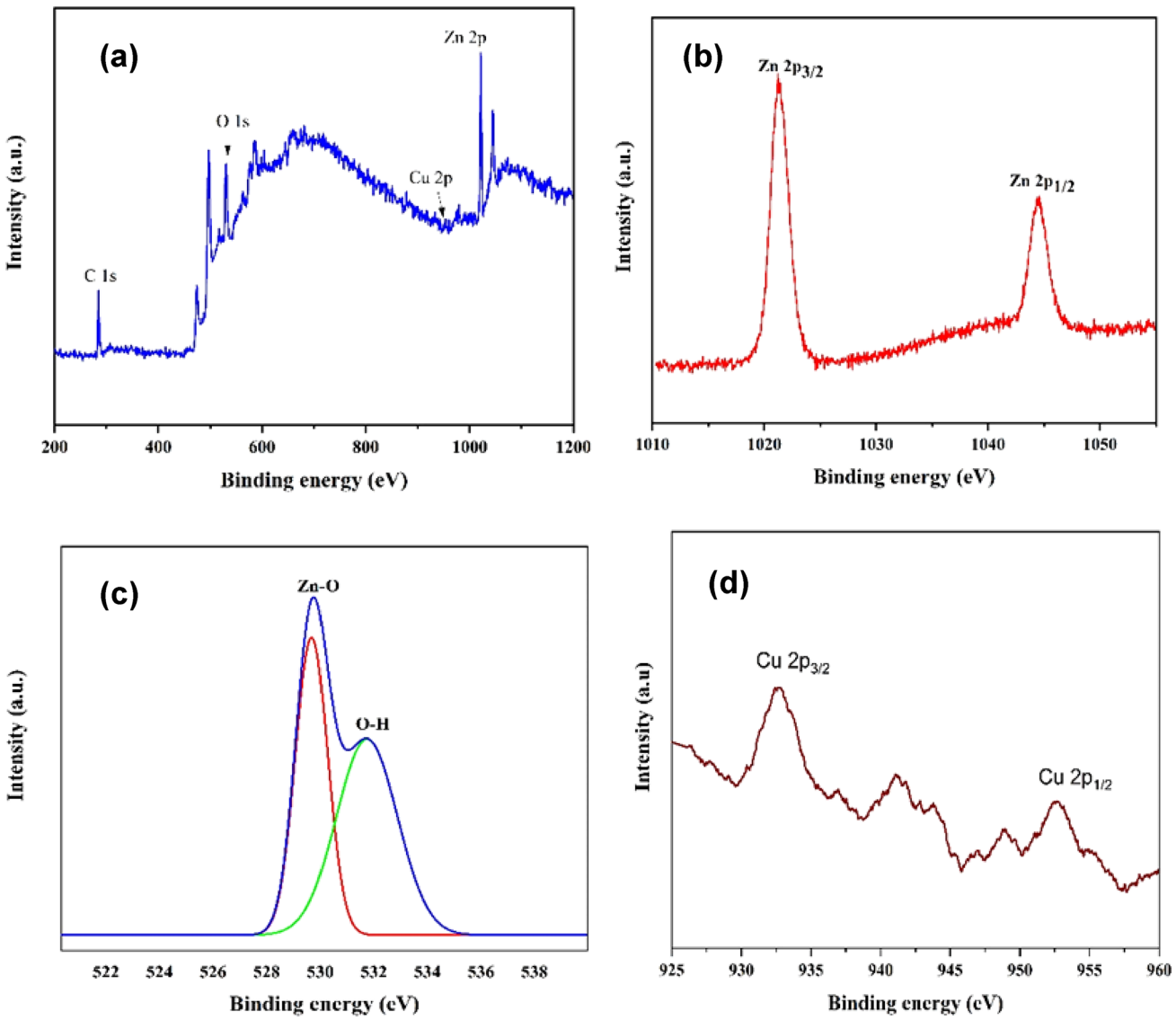

Fig. 7 XPS results obtained for **a** Cu-rGO/ZnO nanocomposite **b** high resolution Zn 2p region, **c** high resolution O1s region and **d** high resolution Cu 2p region

the rapid recombination of the photogenerated excitons, and lower intensity of PL emission indicates a lower rate of recombination (Shenoy et al. 2019). The PL spectra of ZnO show a strong intense peak at 379 nm, correlated to excitonic band–band radiative recombination. The PL spectra of the sample Cu-rGO/ZnO shows an intense peak at 380 nm. The quenching of PL emission is evidence that the recombination of charge carriers was effectively inhibited as a result of the collective influence of Cu and rGO doping with ZnO (Shenoy et al. 2021). In addition, the peak appears at 476 nm (ZnO) and a peak at 477 nm (Cu-rGO/ZnO) due to defect-related emission in nanostructures.

SEM & EDAX

Scanning electron microscopy (SEM) and energy dispersive x-ray analysis (EDAX) provides information on morphology, size and elemental ions of Cu-rGO/ZnO nanocomposites. Figure 5a, b shows the SEM images obtained for CTAB-capped Cu-rGO/ZnO nanocomposites. Figure 5a, b

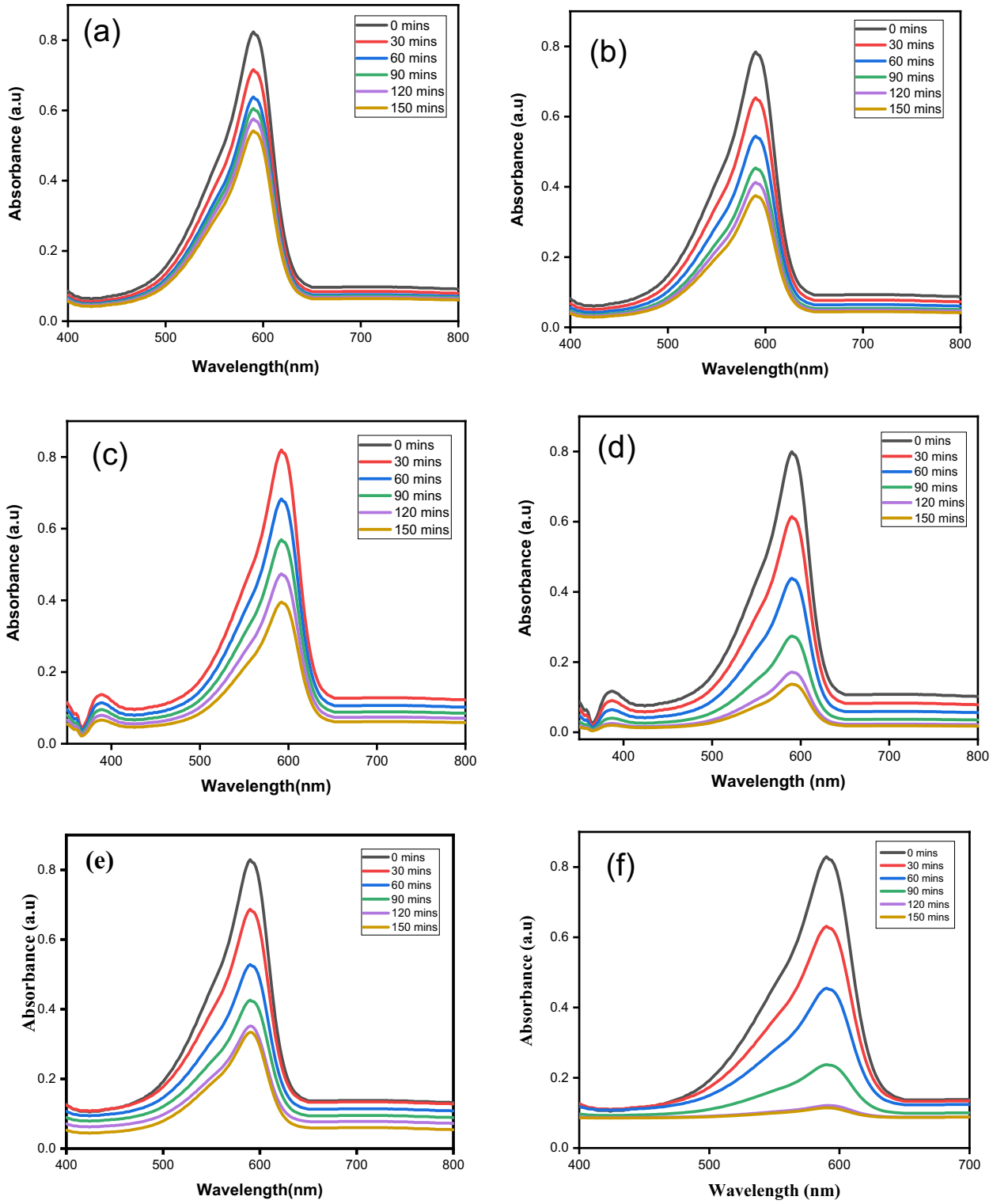

Fig. 8 UV–Vis absorbance spectra obtained for bromophenol blue dye degradation using **a** ZnO 0.01 g/L **b** ZnO 0.1 g/L **c** rGO/ZnO 0.01 g/L **d** rGO/ZnO 0.1 g/L **e** Cu-rGO/ZnO 0.01 g/L and **f** Cu-rGO/ZnO 0.1 g/L and **g** absence of catalyst under 150 min UV irradiation

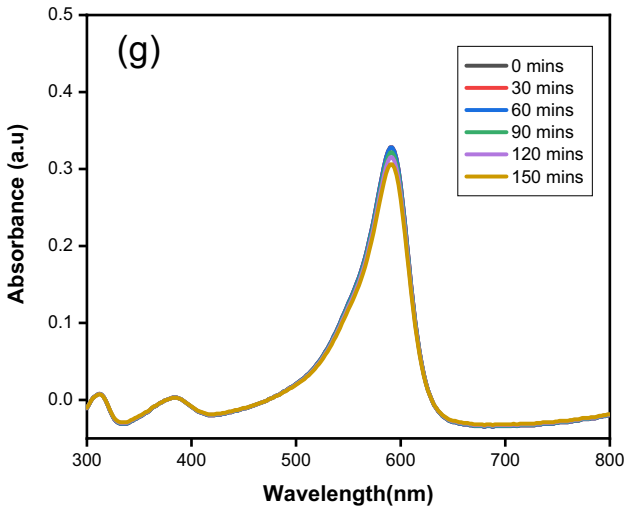

Fig. 8 (continued)

shows that roughly spherical and rod-shaped Cu–ZnO nanoparticles are attached to graphene sheets with less agglomeration. The presence of elemental ions in the composite was evaluated by EDAX analysis. EDAX results are presented in Fig. 5c, which confirms the presence of elements including Cu, Zn, C and O, and the absence of impurities indicates that the synthesis procedure is efficient to prepare impurities-free Cu-rGO/ZnO nanocomposite. The elemental composition of Cu-rGO/ZnO nanocomposite is given in Table 1.

BET analysis

Figure 6a, b shows the BET result obtained for ZnO nanoparticles; it exhibits a type IV loop isotherm with an H1 hysteresis. It is also observed that the ZnO surface was found to be 110 m^2/g. The pore volume and pore radius were found to be 0.166 cc/g and 17.743 Å respectively. Figure 6c, d shows the BET result of Cu-rGO/ZnO nanocomposite. It is noted that Cu-rGO/ZnO nanocomposites exhibit a type IV loop isotherm with an H1 hysteresis loop. It is illustrated that the nanocomposite was mesoporous with a pore radius ranging from 1.5–30 nm. The surface area of Cu-rGO/ZnO nanocomposite was found to be 453 m^2/g and the pore volume of the Cu-rGO/ZnO was found to be 0.688 cc/g. The BET results revealed that the Cu-rGO/ZnO nanocomposites have a large surface area and a high degree of pore size uniformity when compared to ZnO alone.

XPS analysis

The physical attachment of the ternary nanocomposite was evaluated by X-ray photoelectron spectroscopy (XPS). Figure 7 shows the XPS spectra of Cu-rGO/ZnO, which confirms the presence of Zn, O, C and Cu. Full XPS and high-resolution spectra were collected to elucidate the elemental composition present in the prepared nanocomposite. It is noted that peaks observed in Fig. 7a are related to Zn, Cu, O and C ions. Figure 7b shows the characteristic peaks centred at 1022.61 eV (Zn 2p3/2) and 1048.43 eV (Zn 2p1/2), which clearly revealed the oxidation state of zinc. Figure 7c shows the high-resolution O 1 s spectra which show the characteristic peaks centred at 530.69 and 532.51 eV, which are assigned to Zn–O, and C–O bonding (Gonçalves et al. 2020; Madhuvilakku et al. 2017). Figure 7d shows the characteristic peaks at 932.12 eV (Cu 2p3/2) and 952.33 eV (Cu 2p1/2), which revealed the presence of Cu in the composite materials. From the XPS results, it is very clear the prepared nanocomposite is composed of Zn, Cu, O and C atoms.

Photocatalytic degradation of bromophenol blue

Figure 8 shows the UV–Vis absorbance spectra of the photodegradation of bromophenol blue dye solution at different times in the presence of the different photocatalysts. It is clearly indicated that the absorbance intensity decreases as light irradiation time increases. As observed in Fig. 8a and b the percentage of dye degradation is 35 at 150 min in the presence of photocatalyst 0.01 g/L ZnO, whereas the percentage of dye degradation is 52 at 150 min time in the presence of 0.1 g/L ZnO. Figures 8c and d indicate the percentage of dye degradation is 56 at 150 min in the presence of photocatalyst 0.01 g/L rGO/ZnO, whereas the percentage of dye degradation is 83 at 150 min time in the presence of 0.1 g/L rGO/ZnO. Figures 8e and f indicate the percentage of dye degradation is 60 at 150 min in the presence of photocatalyst 0.01 g/L Cu-rGO/ZnO, whereas the percentage of dye degradation is 86 at 150 min time in the presence of 0.1 g/L Cu-rGO/ZnO. The results of Fig. 9 showed that the Cu-rGO/ZnO photocatalyst is degrading the BPB dye slightly faster than the pure ZnO and rGO/ZnO nanocomposite at 150 min. It has clearly shown that the small amount of Cu and rGO incorporated ZnO has greater potential to degrade BPB dye pollutants under UV radiation.

Based on the reported studies, the rate of photocatalytic degradation of dye depends on the nature of the dye, the concentration of dye in water, the nature of the photocatalyst, concentration of photocatalyst, concentration of other compounds in water, temperature, pH, light intensity and wavelength of light etc. (Amakiri et al. Feb. 2022). Figure 8g, shows that BPB dye shows poor degradation at an almost negligible level of 6.7% in the absence of a catalyst under 150 min of UV irradiation. It is noted from Table 2, all the synthesized catalysts have higher degradation performance than pure BPB dye degradation without

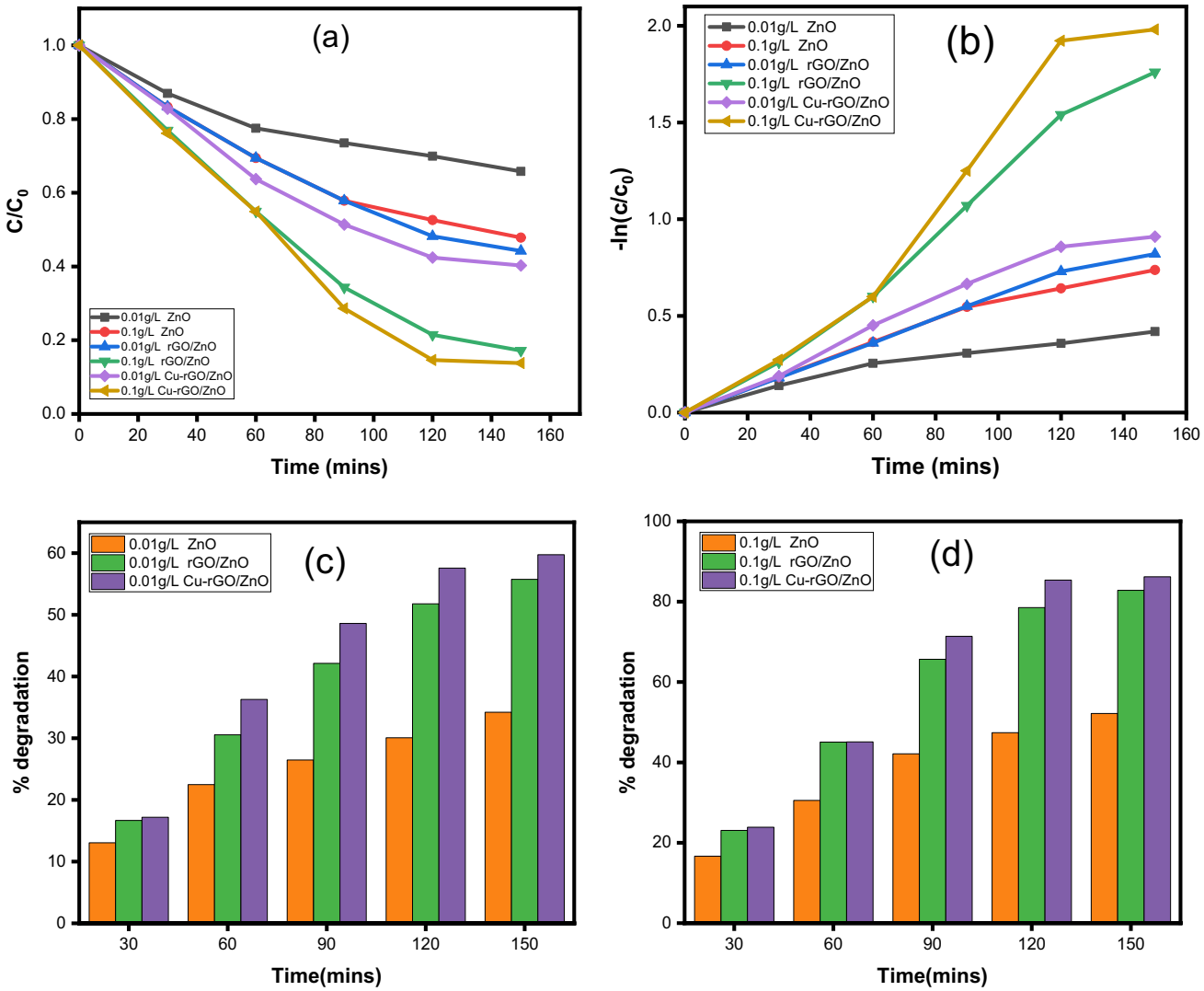

Fig. 9 Photocatalyst performance of different concentrations of ZnO, rGO/ZnO and Cu-rGO/ZnO photocatalysts **a** C/C_0 Vs irradiation time for all samples **b** $-\ln (C/C_0)$ Vs irradiation time plots for all samples **c** and **d** the bar graph plot for degradation efficiency with respect to irradiation time for all samples

Table 2 Rate constant of photocatalytic degradation of different concentrations of ZnO, rGO/ZnO and Cu-rGO/ZnO photocatalysts

Photocatalyst	Concentration	BPB dye initial concentration	% degradation after 150 min	Rate constant
Without catalyst	–	10 ppm	6.68	0.11×10^{-2}
ZnO	0.01 g /L	10 ppm	34.21	0.61×10^{-2}
ZnO	0.1 g /L	10 ppm	52.17	1.15×10^{-2}
rGO/ZnO	0.01 g /L	10 ppm	55.76	1.29×10^{-2}
rGO/ZnO	0.1 g /L	10 ppm	82.83	2.88×10^{-2}
Cu-rGO/ZnO	0.01 g /L	10 ppm	59.74	1.48×10^{-2}
Cu-rGO/ZnO	0.1 g/L	10 ppm	86.21	3.40×10^{-2}

Table 3 Comparison of Cu-rGO/ZnO-based photocatalyst to the previous report against pollutant degradation

Catalyst	Synthesis method	Crystallite size from XRD	Band gap (eV)	Morphology	Experimental conditions			Performance	References
					Catalyst concentration (mg)	Conc. of pollutant	Light	Efficiency (%)	
ZnO-CuO/rGO ternary catalyst	Hydrothermal	ZnO–25.52 nm and ZnO-CuO/rGO–28.80 nm	2.3–2.6 eV	Needle-like ZnO and dot-like CuO are seen at the layered graphene structure	0.1 g	SO_2–2040 mg/m^3, NO–590 mg/m^3	UV–254 nm, 10W	97% desulfurization rate and 64% deNOx	Man et al. (2020)
(ZnO/CuO)/rGO	Solid-state method	Polycrystalline nature	2.8 eV	Flower-like structure	0.1 g	RhB dye solution (100 mL; 5 ppm)	Tungsten lamp (k > 400 nm)-visible light	99% RhB dye and 93% of 4-CP	Kumaresan et al. (2020)
rGO/ CuO/ZnO ternary nanocomposite	Hydrothermal	30.8 nm	–	rGO sheet, spherical CuO and ZnO particles	0.01 g	Phenylhydrazine (1.0 mmol), triethyl phosphite (1.0 mmol)	Blue LED 12 W lamp	95% yield within 2 h	Firoozi and Hosseini-Sarvari (2021)
(rGO-ZnO)/CuO nanocomposite	Microwave-assisted method	Low crystallinity	ZnO–3.09 eV, CuO-ZnO -2.89 eV, rGO-ZnO/CuO–2.43 eV	Random arrays of rod-shaped morphology	20 mg	MB (10 ppm)	A tungsten halogen lamp, 150 W	90% of the initial MB within 105 min	Bekru et al. (2023)
Cu/ZnO/rGO	Two-step hydrothermal method	–	3.20, 3.14, and 2.87 eV for ZnO, Cu/ZnO and Cu/ZnO/rGO, respectively	Nanorods and nanospheres of ZnO and CuO on the rGO nanosheets	2 g/L	Ammonia (NH_4^+–N) 10 mg/L	Xenon (400 nm cutoff filter, visible light region) and Hg lamp (UV light region)	79.2% in UV light and 83.1% under visible light irradiation	He, et al. (2018)
Cu–ZnO/RGO nanocomposite	Microwave-assisted hydrothermal method	–	–	Spherical like particles	20 mg	20 ml MB solution (10 ppm)	UV lamps (UV-c, 256 nm, 40W) A solar simulator (300 W, 5% UV light)	2%	Hsieh and Ting (2018)
ZnO-CuO/rGO ternary composite	Co-precipitation method	The introduction of CuO and rGO in the composite did not change the hexagonal wurtzite structure of ZnO	ZnO–3.16, ZnOCuO–2.85, and ZnO-CuO/rGO–2.62 eV	Spherical metal oxides onto the plate-like graphene	1 g/L	Oily wastewater	Visible light- 75 W	95% after 6 h	Nga et al. Jun. (2022)

Table 3 (continued)

Catalyst	Synthesis method	Crystallite size from XRD	Band gap (eV)	Morphology	Experimental conditions			Performance	References
					Catalyst concentration (mg)	Conc. of pollutant	Light	Efficiency (%)	
Cu-rGO/ZnO nanocomposite	Hydrothermal method	ZnO–54 nm Cu-rGO/ZnO–48 nm	2.94 eV and 3.04 eV for ZnO and the Cu-rGO/ZnO nanocomposite	Roughly spherical and rod-shaped Cu–ZnO nanoparticles are attached to graphene sheets with less agglomeration	0.1 g/L	Bromophenol blue dye (BPB)- 10 ppm	Xe arc lamps, 20 W (with ultraviolet cut-off filter)	95% after 150 min	This work

catalysts. In this study, the higher rate constant is observed as 3.401×10^{-2} min^{-1} for BPB dye degradation using the photocatalyst 0.1 g/L Cu-rGO/ZnO. The significant photocatalytic activity of Cu-rGO/ZnO nanocomposite was achieved due to the incorporation of Cu and rGO into ZnO nanoparticles, enabling improved UV radiation absorption and inhibiting the recombination of photogenerated charges (Rajeshwar et al. 2008). Further, rGO changes the ZnO surface electric charge and is attached physically to ZnO, which causes more adsorption and degradation. The improved adsorption and degradation are due to the zero-charge potential of Cu-rGO/ZnO (pzc-8.6) which is higher than bare ZnO (pzc-7.7). According to Nezamzadeh-Ejhieh et al. at pH lower than pHpzc, the catalyst is more positively charged (Nezamzadeh-Ejhieh and Zabihi-Mobarakeh 2014). Thus, the adsorption of dye molecules (active sulphonate (SO_3^{2-})) on Cu-rGO/ZnO is more than bare ZnO (Trefalt et al. 2011; Nezamzadeh-Ejhieh and Shirzadi 2014).

The characteristic and photocatalytic efficiency of Cu-rGO/ZnO based photocatalyst is presented in Table 3. It shows that the prepared Cu-rGO/ZnO exhibit significant photocatalytic dye degradation efficiency against bromophenol blue.

Antibacterial activity of Cu-rGO/ZnO nanocomposites

The agar well diffusion method was adopted to test the antibacterial activity of Cu-rGO/ZnO nanocomposites against the following pathogens, *Escherichia coli, Staphylococcus aureus, Enterococcus faecium* and *Pseudomonas aeruginosa*. Figure 10 shows the microscopic images of the antibacterial activity of ZnO nanoparticle against (a) *Enterococcus faecium* (b) *Staphylococcus aureus* (c) *Pseudomonas aeruginosa* (d) *Escherichia coli* and Cu-rGO/ZnO nanocomposite against (e) *Staphylococcus aureus* (f) *Enterococcus faecium* (g) *Escherichia coli*, (h) *Pseudomonas aeruginosa*. The results revealed that both ZnO nanoparticles and Cu-rGO/ZnO nanocomposite exhibited potential antibacterial effects by suppressing microbial growth against gram-positive and gram-negative bacteria. The maximum zones of inhibition were found for the nanocomposite concentrations of up to 200 µg/ml. The significant antibacterial effect of the nanoparticles can be correlated with many factors such as type of bacteria, type of the nanocomposite, dosage of nanocomposite and synthesizing methods.

From the zones of inhibition values from Table 4 and Fig. 11, it is observed that Gram-negative bacterial strains are more susceptible to ZnO-NPs and Cu-rGO/ZnO

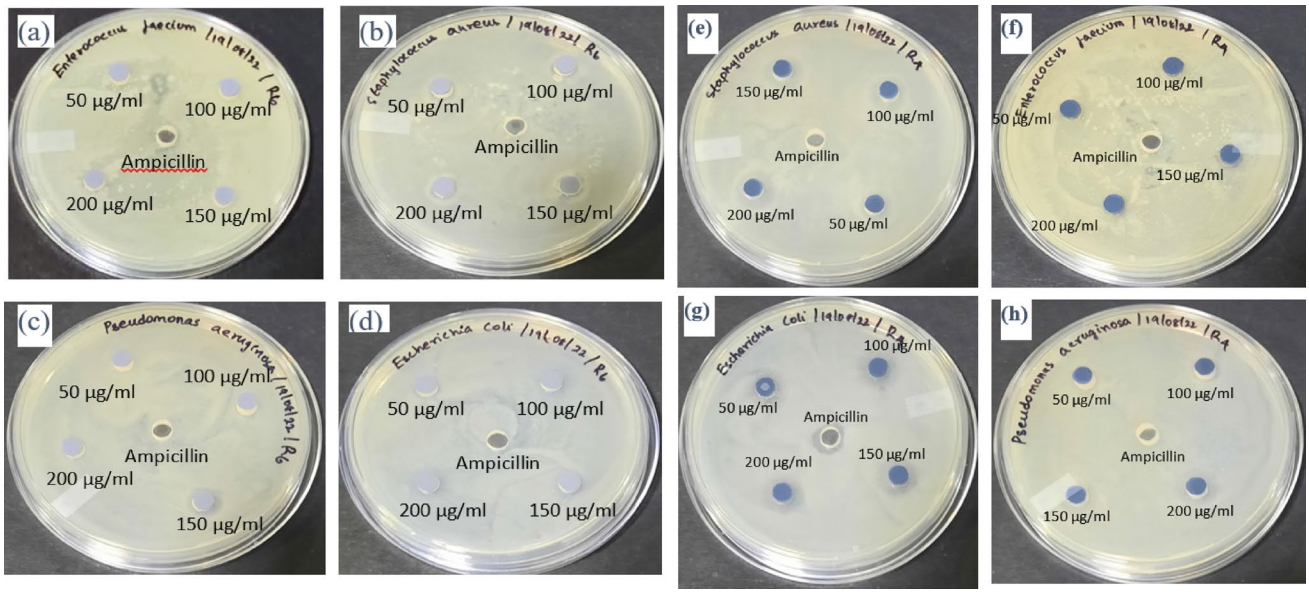

Fig. 10 Microscopic images of the antibacterial activity of ZnO nanoparticle against **a** *Enterococcus faecium* **b** *Staphylococcus aureus* **c** *Pseudomonas aeruginosa* **d** *Escherichia coli* and Cu-rGO/ZnO nanocomposite against **e** *Staphylococcus aureus* **f** *Enterococcus faecium* **g** *Escherichia coli,* **h** *Pseudomonas aeruginosa*

nanocomposite as compared to Gram-positive bacterial strains. For ZnO-NPs; gram-positive microbes, *S. aureus* forms a ZOI of 7.5 ± 0.4 mm, whereas E.facium form a ZOI of 3.5 ± 0.15 mm at 200 µg/ml concentration and gram-negative microbes, *E. coli* display 8.5 ± 0.43 mm ZOI, whereas P.aeruginosa forms 9.5 ± 0.48 mm ZOI at 200 µg/ml concentration. For Cu-rGO/ZnO nanocomposite, gram-positive microbes, *S. aureus* forms a ZOI of 10.5 ± 0.06 mm, whereas *E. facium* form a ZOI of 8.5 ± 0.43 mm at 200 µg/ml concentration and gram-negative microbes, *E. coli* display 11.1 ± 0.01 mm ZOI, whereas *P. aeruginosa* forms 14 ± 0.01 mm ZOI at 150 µg/ml concentration.

The results confirm that Cu-rGO/ZnO nanocomposite exhibits better antibacterial activity than pure ZnO nanoparticles. The Cu-rGO/ZnO nanocomposite concentration of 150 µg/ml exhibits a maximum zone of inhibition against P.Aeruginosa and E.Coli, indicating the nanocomposite was found to be significant antibacterial action in a dose-dependent manner. The mechanism of antibacterial

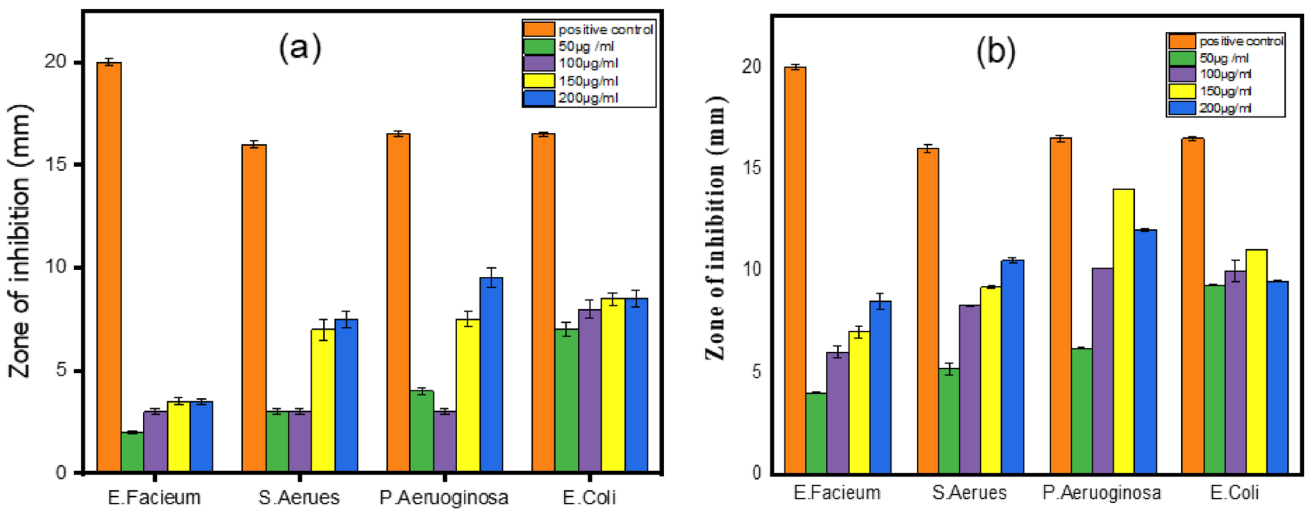

Fig. 11 Zone of inhibition (mm) produced by **a** ZnO against gram-positive and gram-negative bacteria and **b** Cu-rGO/ZnO nanocomposite against gram-positive and gram-negative bacteria

Table 4 Antibacterial activity (Zone of inhibition in mm) of ZnO NPs and Cu-rGO/ZnO nanocomposite

	E. facium					*S. aureus*				
	Positive control	50 µg/ml	100 µg/ml	150 µg/ml	200 µg/ml	Positive control	50 µg/ml	100 µg/ml	150 µg/ml	200 µg/ml
ZnO	20 ± 0.15	2 ± 0.1	3 ± 0.15	3.5 ± 0.18	3.5 ± 0.15	16 ± 0.2	3 ± 0.5	3 ± 0.15	7 ± 0.5	7.5 ± 0.4
Cu-rGO/ZnO	20 ± 0.15	4 ± 0.2	6 ± 0.3	7 ± 0.15	8.5 ± 0.43	16 ± 0.2	5.2 ± 0.03	8.3 ± 0.04	9.2 ± 0.05	10.5 ± 0.06
	P. aeruginosa					*E. coli*				
ZnO	16.5 ± 0.15	4 ± 0.2	3 ± 01.5	7.5 ± 0.38	9.5 ± 0.48	16.5 ± 0.1	7 ± 0.35	8 ± 0.45	8.5 ± 0.3	8.5 ± 0.43
Cu-rGO/ZnO	16.5 ± 0.15	6.2 ± 0.05	10.1 ± 0.01	14 ± 0.01	12 ± 0.05	16.5 ± 0.1	9.3 ± 0.05	10 ± 0.05	11.1 ± 0.01	9.5 ± 0.04

activity of the nanocomposite was attributed to a combination of direct destruction of the cell membrane by the Cu-rGO/ZnO nanocomposite, the generation of reactive oxygen species by Cu-rGO/ZnO entities, and accumulation of the nanocomposite on cell cytoplasm (Zhu et al. 2013; Cai et al. 2011; Ghosh and Das 2015; Yang et al. 2009; El-Shafai et al. 2019; Khalid et al. May 2021).

Conclusion

A ternary nanocomposite was successfully prepared using the hydrothermal method. The XRD pattern revealed that the prepared samples exhibited the hexagonal wurtzite structure. UV–Vis absorbance showed that the maximum absorption was observed at 374 nm and 368 nm for ZnO and the Cu-rGO/ZnO nanocomposite due to the large exciton binding energy of the bulk ZnO at room temperature. Scanning electron microscopy revealed that roughly spherical rod shaped Cu–ZnO nanoparticles were attached to the rGO sheets. EDAX analysis confirmed that the prepared sample was free of impurities. The surface area of the Cu-rGO/ZnO nanocomposite was found to be 453.1 m^2/g and the pore volume of the Cu-rGO/ZnO was found to be 0.688 cc/g as inferred from BET analysis. The photocatalytic dye degradation of Cu-rGO/ZnO was improved by the addition of Cu and rGO. The band gap widening by Cu doping and efficient electron hole separation induced by rGO were responsible for enhanced photocatalytic activity of Cu-rGO/ZnO. The Cu-rGO/ZnO nanocomposite exhibited significant antibacterial activity in a dose dependent manner. The rGO sheets enabled the increased reactive surface area for the growth of ZnO on it.

Data availability Not applicable.

Declarations

Conflict of interest All authors declared that there is no conflict of interest.

Ethical approval This article does not contain any studies with human or animal subjects.

References

Amakiri KT, Angelis-Dimakis A, Canon AR (2022) Recent advances, influencing factors, and future research prospects using photocatalytic process for produced water treatment. Water Sci Technol 85(3):769–788. https://doi.org/10.2166/wst.2021.641

Arora AK, Jaswal VS, Singh K, Singh R (2016) Applications of metal/mixed metal oxides as photocatalyst: (a review). Orient J Chem 32(4):2035

Asgharian M, Mehdipourghazi M, Khoshandam B, Keramati N (2019) Photocatalytic degradation of methylene blue with synthesized rGO/ZnO/Cu. Chem Phys Lett 719:1–7. https://doi.org/10.1016/j.cplett.2019.01.037

Baizaee SM, Arabi M, Bahador AR (2018) A simple, one-pot, low temperature and pressure route for the synthesis of RGO/ZnO nanocomposite and investigating its photocatalytic activity. Mater Sci Semicond Process 82:135–142

Balasubramani V, Sureshkumar S, Rao TS, Sridhar TM (2019) Impedance spectroscopy-based reduced graphene oxide-incorporated ZnO composite sensor for H_2S investigations. ACS Omega 4(6):9976–9982. https://doi.org/10.1021/acsomega.9b00754

Bayramoglu G, Kunduzcu G, Arica MY (2020) Preparation and characterization of strong cation exchange terpolymer resin as effective adsorbent for removal of disperse dyes. Polym Eng Sci 60(1):192–201

Bekru A, Tufa LT, Zelekew OA, Gwak J, Lee J, Sabir F (2023) Microwave-assisted synthesis of rGO-ZnO/CuO nanocomposites for photocatalytic degradation of organic pollutants. Crystals (basel) 13:133. https://doi.org/10.3390/cryst13010133

Bolaghi ZK, Masoudpanah SM, Hasheminiasari M (2019) Photocatalytic activity of ZnO/RGO composite synthesized by one-pot solution combustion method. Mater Res Bull 115:191–195

Bramhaiah K, Singh VN, John NS (2016) Hybrid materials of ZnO nanostructures with reduced graphene oxide and gold nanoparticles: enhanced photodegradation rates in relation to their composition and morphology. Phys Chem Chem Phys 18(3):1478–1486. https://doi.org/10.1039/C5CP05081B

Cai X et al (2011) Synergistic antibacterial brilliant blue/reduced graphene oxide/quaternary phosphonium salt composite with excellent water solubility and specific targeting capability. Langmuir 27(12):7828–7835. https://doi.org/10.1021/la201499s

Chadha U et al (2022) A review of the function of using carbon nanomaterials in membrane filtration for contaminant removal from wastewater. Mater Res Express 9(1):12003

Chiam S-L, Pung S-Y, Yeoh F-Y (2020) Recent developments in MnO2-based photocatalysts for organic dye removal: a review. Environ Sci Pollut Res 27:5759–5778

Danish MSS et al (2021) Photocatalytic applications of metal oxides for sustainable environmental remediation. Metals (basel) 11(1):80

Dědková K et al (2015) ZnO/graphite composites and its antibacterial activity at different conditions. J Photochem Photobiol B 151:256–263

El-Shafai N, El-Khouly ME, El-Kemary M, Ramadan M, Eldesoukey I, Masoud M (2019) Graphene oxide decorated with zinc oxide nanoflower, silver and titanium dioxide nanoparticles: fabrication, characterization, DNA interaction, and antibacterial activity. RSC Adv 9(7):3704–3714

Etacheri V, Roshan R, Kumar V (2012) Mg-doped ZnO nanoparticles for efficient sunlight-driven photocatalysis. ACS Appl Mater Interfaces 4(5):2717–2725. https://doi.org/10.1021/am300359h

Firoozi S, Hosseini-Sarvari M (2021) Visible-light-induced C-P-bond formation using reduced graphene oxide decorated with copper oxide/zinc oxide (rGO/CuO/ZnO) as ternary recyclable nanophotocatalyst. ChemistrySelect 6(8):1764–1771. https://doi.org/10.1002/slct.202004411

Ganachari SV, Hublikar L, Yaradoddi JS, Math SS (2019) Metal oxide nanomaterials for environmental applications. Hand Ecomater 4:2357–2368

Gang R, Xu L, Xia Y, Zhang L, Wang S, Li R (2021) Facile one-step production of 2D/2D ZnO/rGO nanocomposites under microwave irradiation for photocatalytic removal of tetracycline. ACS Omega 6:3831–3839

Gautam S et al (2020) Metal oxides and metal organic frameworks for the photocatalytic degradation: a review. J Environ Chem Eng 8(3):103726

Ghosh S, Das AP (2015) Modified titanium oxide (TiO_2) nanocomposites and its array of applications: a review. Toxicol Environ Chem 97(5):491–514

Gonçalves AHA, Siciliano PHC, Alves OC, Cesar DV, Henriques CA, Gaspar AB (2020) Synthesis of a magnetic Fe3O4/RGO composite for the rapid photo-fenton discoloration of indigo carmine dye. Top Catal 63(11):1017–1029. https://doi.org/10.1007/s11244-020-01277-0

Guo H-L, Wang X-F, Qian Q-Y, Wang F-B, Xia X-H (2009) A green approach to the synthesis of graphene nanosheets. ACS Nano 3(9):2653–2659. https://doi.org/10.1021/nn900227d

He S et al (2018) High efficient visible-light photocatalytic performance of Cu/ZnO/rGO nanocomposite for decomposing of aqueous ammonia and treatment of domestic wastewater. Front Chem. https://doi.org/10.3389/fchem.2018.00219

Herng TS et al (2007) Magnetic anisotropy in the ferromagnetic Cu-doped ZnO nanoneedles. Appl Phys Lett 90(3):032509. https://doi.org/10.1063/1.2433028

Hsieh S-H, Ting J-M (2018) Characterization and photocatalytic performance of ternary Cu-doped ZnO/Graphene materials. Appl Surf Sci 427:465–475. https://doi.org/10.1016/j.apsusc.2017.06.176

Hummers WS Jr, Offeman RE (1958) Preparation of graphitic oxide. J Am Chem Soc 80(6):1339

Jagadeeshan S, Parsanathan R (2019) Nano-metal oxides for antibacterial activity. In: Naushad M, Rajendran S, Gracia F (eds) Advanced nanostructured materials for environmental remediation. Environmental chemistry for a sustainable world, vol 25. Springer, Cham

Janotti A, Van de Walle CG (2009) Fundamentals of zinc oxide as a semiconductor. Rep Prog Phys 72(12):126501. https://doi.org/10.1088/0034-4885/72/12/126501

Jothimani B, Sureshkumar S, Venkatachalapathy B (2017) Synthesis and characterization of surface modified, fluorescent and biocompatible ZnS nanoparticles with a hydrophobic chitosan derivative. J Fluoresc. https://doi.org/10.1007/s10895-017-2059-5

Kavitha MK, Gopinath P, John H (2015) Reduced graphene oxide–ZnO self-assembled films: tailoring the visible light photoconductivity by the intrinsic defect states in ZnO. Phys Chem Chem Phys 17(22):14647–14655. https://doi.org/10.1039/C5CP01318F

Khalid A et al (2021) Synergistic effects of Cu-doped ZnO nanoantibiotic against Gram-positive bacterial strains. PLoS ONE. https://doi.org/10.1371/journal.pone.0251082

Khurshid F, Jeyavelan M, Hudson MSL, Nagarajan S (2019) Ag-doped ZnO nanorods embedded reduced graphene oxide nanocomposite for photo-electrochemical applications. R Soc Open Sci 6(2):181764. https://doi.org/10.1098/rsos.181764

Kumar R, Chawla J (2014) Removal of cadmium ion from water/wastewater by nano-metal oxides: a review. Water Qual Expo Health 5:215–226

Kumar P, Som S, Pandey MK, Das S, Chanda A, Singh J (2018) Investigations on optical properties of ZnO decorated graphene oxide (ZnO@GO) and reduced graphene oxide (ZnO@r-GO). J Alloys Compd 744:64–74. https://doi.org/10.1016/j.jallcom.2018.02.057

Kumaresan N, Sinthiya MMA, Ramamurthi K, Ramesh Babu R, Sethuraman K (2020) Visible light driven photocatalytic activity of ZnO/CuO nanocomposites coupled with rGO heterostructures synthesized by solid-state method for RhB dye degradation. Arab J Chem 13(2):3910–3928. https://doi.org/10.1016/j.arabjc.2019.03.002

Madhuvilakku R, Alagar S, Mariappan R, Piraman S (2017) Green one-pot synthesis of flowers-like Fe3O4/rGO hybrid nanocomposites for effective electrochemical detection of riboflavin and low-cost supercapacitor applications. Sens Actuators B Chem 253:879–892. https://doi.org/10.1016/j.snb.2017.06.126

Man H, Wen C, Luo W, Bian J, Wang W, Li C (2020) Simultaneous deSOx and deNOx of marine vessels flue gas on ZnO-CuO/rGO: Photocatalytic oxidation kinetics. J Ind Eng Chem 92:77–87. https://doi.org/10.1016/j.jiec.2020.08.022

Mandal SK et al (2019) Engineering of ZnO/rGO nanocomposite photocatalyst towards rapid degradation of toxic dyes. Mater Chem Phys 223:456–465. https://doi.org/10.1016/j.matchemphys.2018.11.002

Meshram SP, Adhyapak PV, Amalnerkar DP, Mulla IS (2016) Cu doped ZnO microballs as effective sunlight driven photocatalyst. Ceram Int 42(6):7482–7489. https://doi.org/10.1016/j.ceramint.2016.01.154

Mohamed HH, Mohamed SK (2018) Rutile TiO_2 nanorods/MWCNT composites for enhanced simultaneous photocatalytic oxidation of organic dyes and reduction of metal ions. Mater Res Express 5(1):15057. https://doi.org/10.1088/2053-1591/aaa73b

Mohammad A, Ahmad K, Rajak R, Mobin SM (2017) Binder free modifcation of glassy carbon electrode by employing reduced graphene oxide/ZnO composite for voltammetric determination of certain nitroaromatics. Electroanalysis 29:1–10

Mohammad A, Ahmad K, Qureshi A, Tauqeer M, Mobin SM (2018) Zinc oxide-graphitic carbon nitride nanohybrid as an efficient electrochemical sensor and photocatalyst. Sens Actuators B Chem 277:467–476

Nezamzadeh-Ejhieh A, Shirzadi A (2014) Enhancement of the photocatalytic activity of ferrous oxide by doping onto the nanoclinoptilolite particles towards photodegradation of tetracycline. Chemosphere 107:136–144

Nezamzadeh-Ejhieh A, Zabihi-Mobarakeh H (2014) Heterogeneous photodecolorization of mixture of methylene blue and bromophenol blue using CuO-nano-clinoptilolite. J Ind Eng Chem 20(4):1421–1431

Nga PTT, Duc NM, Van Minh N, Lien NH (2022) Photocatalytic degradation of oily wastewater over ZnO-CuO/rGO photocatalyst under visible light. Vietnam J Chem 60(3):389–397. https://doi.org/10.1002/vjch.202100171

Peng Y, Ji J, Chen D (2015) Ultrasound assisted synthesis of ZnO/reduced graphene oxide composites with enhanced photocatalytic activity and anti-photocorrosion. Appl Surf Sci 356:762–768

Pirhashemi M, Habibi-Yangjeh A, Rahim Pouran S (2018) Review on the criteria anticipated for the fabrication of highly efficient ZnO-based visible-light-driven photocatalysts. J Ind Eng Chem 62:1–25. https://doi.org/10.1016/j.jiec.2018.01.012

Rajeshwar K et al (2008) Heterogeneous photocatalytic treatment of organic dyes in air and aqueous media. J Photochem Photobiol, C 9(4):171–192. https://doi.org/10.1016/j.jphotochemrev.2008.09.001

Ramos PG, Flores E, Luyo C, Sánchez LA, Rodriguez J (2019) Fabrication of ZnO-RGO nanorods by electrospinning assisted hydrothermal method with enhanced photocatalytic activity. Mater Today Commun 19:407–412

Ravichandran K, Chidhambaram N, Gobalakrishnan S (2016) Copper and graphene activated ZnO nanopowders for enhanced photocatalytic and antibacterial activities. J Phys Chem Solids 93:82–90. https://doi.org/10.1016/j.jpcs.2016.02.013

Sampaio MJ et al (2015) Synergistic effect between carbon nanomaterials and ZnO for photocatalytic water decontamination. J Catal 331:172–180. https://doi.org/10.1016/j.jcat.2015.08.011

Sengunthar P, Bhavsar KH, Balasubramanian C, Joshi US (2020) Physical properties and enhanced photocatalytic activity of ZnO-rGO nanocomposites. Appl Phys A 126:1–9

Sernelius BE, Berggren K-F, Jin Z-C, Hamberg I, Granqvist CG (1988) Band-gap tailoring of ZnO by means of heavy Al doping. Phys Rev B 37(17):10244–10248. https://doi.org/10.1103/PhysRevB.37.10244

Shenoy S, Jang E, Park TJ, Gopinath CS, Sridharan K (2019) Cadmium sulfide nanostructures: Influence of morphology on the photocatalytic degradation of erioglaucine and hydrogen generation. Appl Surf Sci 483:696–705. https://doi.org/10.1016/j.apsusc.2019.04.018

Shenoy S, Ahmed S, Lo IMC, Singh S, Sridharan K (2021) Rapid sonochemical synthesis of copper doped ZnO grafted on graphene as a multi-component hierarchically structured visible-light-driven photocatalyst. Mater Res Bull 140:111290. https://doi.org/10.1016/j.materresbull.2021.111290

Silva CG, Faria JL (2009) Effect of key operational parameters on the photocatalytic oxidation of phenol by nanocrystalline sol–gel TiO_2 under UV irradiation. J Mol Catal A Chem 305(1):147–154. https://doi.org/10.1016/j.molcata.2008.12.015

Srinet G, Kumar R, Sajal V (2013) Effects of Ni doping on structural, optical and dielectric properties of ZnO. Ceram Int 39(7):7557–7561. https://doi.org/10.1016/j.ceramint.2013.03.008

Sureshkumar S, Venkatachalapathy B, Sridhar TM (2019) Enhanced H_2S gas sensing properties of Mn doped ZnO nanoparticles—an impedance spectroscopic investigation. Mater Res Express. https://doi.org/10.1088/2053-1591/ab0eef

Thennarasu G, Sivasamy A (2016) Enhanced visible photocatalytic activity of cotton ball like nano structured Cu doped ZnO for the degradation of organic pollutant. Ecotoxicol Environ Saf 134:412–420

Trefalt G, Malic B, Kuscer D, Holc J, Kosec M (2011) Synthesis of $Pb(Mg_{1/3}Nb_{2/3})O_3$ by self-assembled colloidal aggregates. J Am Ceram Soc 94(9):2846–2856. https://doi.org/10.1111/j.1551-2916.2011.04443.x

Ullah H, Mushtaq L, Ullah Z, Fazal A, Khan AM (2021) Effect of vegetable waste extract on microstructure, morphology, and photocatalytic efficiency of ZnO–CuO nanocomposites. Inorg Nano-Metal Chem 51(7):963–975. https://doi.org/10.1080/24701556.2020.1813766

Vink TJ, Overwijk MHF, Walrave W (1996) The active dopant concentration in ion implanted indium tin oxide thin films. J Appl Phys 80(7):3734–3738. https://doi.org/10.1063/1.363324

Wu H, Lin S, Chen C, Liang W, Liu X, Yang H (2016) A new ZnO/rGO/polyaniline ternary nanocomposite as photocatalyst with improved photocatalytic activity. Mater Res Bull 83:434–441

Xue B, Zou Y (2018) High photocatalytic activity of ZnO–graphene composite. J Colloid Interface Sci 529:306–313

Yang H, Liu C, Yang D, Zhang H, Xi Z (2009) Comparative study of cytotoxicity, oxidative stress and genotoxicity induced by four typical nanomaterials: the role of particle size, shape and composition. J Appl Toxicol 29(1):69–78

Zhang T-Y, Zhang D (2011) Aqueous colloids of graphene oxide nanosheets by exfoliation of graphite oxide without ultrasonication. Bull Mater Sci 34(1):25–28. https://doi.org/10.1007/s12034-011-0048-x

Zhang A, Gu Z, Chen W, Li Q, Jiang G (2018) Removal of refractory organic pollutants in reverse-osmosis concentrated leachate by microwave-fenton process. Environ Sci Pollut Res 25:28907–28916

Zhu Z, Su M, Ma L, Ma L, Liu D, Wang Z (2013) Preparation of graphene oxide–silver nanoparticle nanohybrids with highly antibacterial capability. Talanta 117:449–455

Publisher's Note Springer Nature remains neutral with regard to jurisdictional claims in published maps and institutional affiliations.

Springer Nature or its licensor (e.g. a society or other partner) holds exclusive rights to this article under a publishing agreement with the author(s) or other rightsholder(s); author self-archiving of the accepted manuscript version of this article is solely governed by the terms of such publishing agreement and applicable law.